Multipolar analysis of second-harmonic generation in (111) Gallium Arsenide nanoparticles

IOP Conf. Series: Journal of Physics: Conf. Series **1461** (2020) 012185 doi:10.1088/1742-6596/1461/1/012185

Multipolar analysis of second-harmonic generation in (111) Gallium Arsenide nanoparticles

I Volkovskaya[1], D Smirnova[1], L Xu[2], J Sautter[3,4], A Miroshnichenko[2], M Lysevych[5], R Camacho-Morales[3], K Z Kamali[3], F Karouta[5], K Vora[5], H H Tan[5], M Kauranen[6], I Staude[4], C Jagadish[5], D Neshev[3] and M Rahmani[3]

[1] Institute of Applied Physics, Russian Academy of Sciences, Nizhny Novgorod 603950, Russia
[2] School of Engineering and Information Technology, University of New South Wales, Canberra, ACT 2600, Australia
[3] Nonlinear Physics Centre, Research School of Physics and Engineering, The Australian National University, Canberra, ACT 2601 Australia
[4] Institute of Applied Physics, Abbe Center of Photonics, Friedrich Schiller University Jena, 07745 Jena, Germany
[5] Department of Electronic Materials Engineering, Research School of Physics and Engineering, The Australian National University, Canberra, ACT 2601, Australia
[6] Optics Laboratory, Institute of Physics, Tampere University of Technology, P.O. Box 692, FI-33101 Tampere, Finland

E-mail: volkovskaya@appl.sci-nnov.ru

Abstract. We perform multipolar analysis of second-harmonic generation (SHG) from (111)-grown gallium arsenide (GaAs) nanoantennas and discuss its specifics. It was experimentally demonstrated that the conversion efficiency in axially-symmetric (111) GaAs nanoparticles remains constant under the polarization rotation of normally incident radiation in a wide range of particle sizes, while the SHG radiation pattern changes. We apply the analytical method based on the Lorentz lemma to explain this behaviour. The induced nonlinear current is decomposed into two rotating contributions, which are shown to generate multipoles of different parities. Thus, the total SHG intensity in the far-field is proved to be independent of the in-plane rotation of the pump polarization. Nevertheless, due to the threefold symmetry of the crystal with regard to the (111) direction, the SHG radiation pattern rotates around the polar axis repeating its shape every 60°.

1. Introduction

Dielectric nanoparticles have recently emerged as a platform for low-loss multipolar nonlinear nanophotonics (1). The group of III-V semiconductors is considered promising for applications in nonlinear nanoantennas since it contains materials possessing relatively high refractive indices, low Ohmic losses in the near infrared (NIR), and strong second-order bulk nonlinearity (2).

Here, we describe features of SHG from (111)-grown GaAs nanoantennas. We identify multipolar nonlinear sources induced in GaAs nanoparticles and analyze their redistribution rotating the in-plane pump polarization. With the use of the developed description based on the Lorentz lemma (2; 3), we explain the experimentally observed polarization-independent nonlinear conversion efficiency and rotation of SHG radiation pattern.

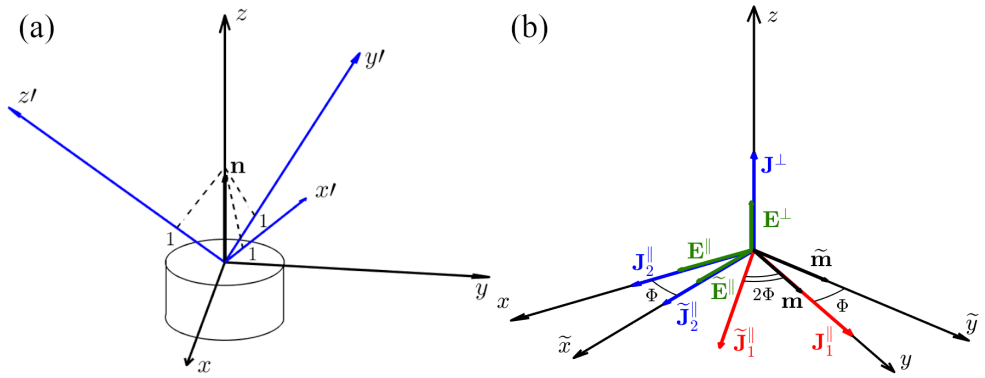

Figure 1. (a) Crystalline and laboratory coordinate systems. The disk-shaped particle is grown along the (111) normal **n**. (b) Scheme of the nonlinear source rotation in the case of single-mode approximation. The FW field inside the particle is assumed to be described by the magnetic dipole mode with magnetic moment **m**.

2. Nonlinear polarization sources

GaAs material possesses a zinc-blende structure, hence, its second-order susceptibility tesnor has only three nonvanishing components $\chi^{(2)}_{x'y'z'}$, $\chi^{(2)}_{y'z'x'}$ and $\chi^{(2)}_{z'x'y'}$, where x', y', z' refer to the principal-axis system of the crystal. The induced nonlinear current is then defined as $J_i^{'(2\omega)} = 2i\omega\varepsilon_0\chi^{(2)}_{ijk}E'_jE'_k$. For a nanodisk which is grown along the (111) direction, one needs to perform the appropriate coordinate transformation between the crystal and laboratory frames (see Fig. 1(a)). The transformation matrix can be expressed through the multiplication of the rotation matrices with three Euler angles α, β, γ: $\hat{T} = \hat{R}(\alpha,\mathbf{e}_z)\hat{R}(\beta,\mathbf{e}_x)\hat{R}(\gamma,\mathbf{e}_z)$, where $\alpha = 0$, $\beta = \tan^{-1}\sqrt{2}$, $\gamma = \pi/4$. For a given electric field $\mathbf{E}$ in the laboratory Cartesian coordinate system (x,y,z), the corresponding field in the crystalline coordinate system is found as $\mathbf{E}' = \hat{T}\mathbf{E}$. Using $\mathbf{J} = \hat{T}^{-1}\mathbf{J}'$, we obtain explicit expressions for the nonlinear current induced at the second-harmonic frequency in the laboratory Cartesian coordinate system and decompose it into two contributions $\mathbf{J}(2\omega) = \mathbf{J}^{\parallel}(2\omega) + \mathbf{J}^{\perp}(2\omega)$, where the out-of-plane current is given by

$$J^{\perp}(2\omega) \equiv J_z(2\omega) = 4i\omega\varepsilon_0 d_{36}\left(-\frac{1}{\sqrt{6}}\left(E_x^2(\omega)+E_y^2(\omega)\right)+\frac{1}{\sqrt{3}}E_z^2(\omega)\right), \tag{1}$$

and the in-plane current is represented as a sum, $\mathbf{J}^{\parallel}(2\omega) = \mathbf{J}^{\parallel}_1(2\omega) + \mathbf{J}^{\parallel}_2(2\omega)$,

$$\begin{aligned}\mathbf{J}^{\parallel}_1(2\omega) &= \left(J^{\parallel}_{1x}, J^{\parallel}_{1y}\right) = 4i\omega\varepsilon_0 d_{36}\left(\sqrt{\tfrac{2}{3}}E_x(\omega)E_y(\omega), \tfrac{1}{\sqrt{6}}\left(E_x^2(\omega)-E_y^2(\omega)\right)\right),\\ \mathbf{J}^{\parallel}_2(2\omega) &= \left(J^{\parallel}_{2x}, J^{\parallel}_{2y}\right) = 4i\omega\varepsilon_0 d_{36}\left(-\tfrac{1}{\sqrt{3}}E_x(\omega)E_z(\omega), -\tfrac{1}{\sqrt{3}}E_y(\omega)E_z(\omega)\right).\end{aligned} \tag{2}$$

Figure 1(b) exemplifies evolution of the induced nonlinear currents under rotation of the fundamental-wavelength (FW) field structure in-plane by angle Φ. The rotated coordinate system is denoted by tildes. Based on Eqs. (1) and (2), we obtain that the expressions for $\mathbf{J}^{\parallel}_2(2\omega)$ and $\mathbf{J}^{\perp}(2\omega)$ are the same in the original and the rotated coordinate systems, while current $\mathbf{J}^{\parallel}_1(2\omega)$ gets rotated by (-3Φ).

3. Nonlinearly generated multipoles

Next, we determine multipolar composition of the generated SH field. From the above considerations, it is enough to perform calculations in one fixed coordinate system. The multipolar coefficients $a_{E,M}(l,m)$

of SH-generated field can be found using the Lorentz lemma following the procedure described in Refs. (2; 3). These coefficients are determined by the overlap integrals of the nonlinear current $\mathbf{J}(2\omega)$ with vector spherical harmonics $\mathbf{X}_{l,m}(\theta,\varphi)$ and transmission coefficients $t_l^{E,M}$(see Ref. (3)) of the spherical wave irradiating the particle:

$$\begin{aligned} a_E(l,m) &\sim t_l^E \iiint \mathbf{J}(2\omega)\nabla\times\left(j_l(2k_0\sqrt{\varepsilon(2\omega)}r)\mathbf{X}^*_{l,m}(\theta,\varphi)\right)dV, \\ a_M(l,m) &\sim t_l^M \iiint \mathbf{J}(2\omega)j_l(2k_0\sqrt{\varepsilon(2\omega)}r)\mathbf{X}^*_{l,m}(\theta,\varphi)dV. \end{aligned} \tag{3}$$

To simplify derivations, here we consider a spherical nanoparticle excited by x-polarized plane wave. Expressions for the electric field of the incident wave $\mathbf{E}_i = E_0 e^{ik_0 z}\hat{\mathbf{x}}$ and for the electric field inside the nanoparticle $\mathbf{E}_{in}$ in terms of vector spherical harmonics contain functions with $m = \pm 1$ only. Similar reasoning and calculations can be carried out for the disk-shaped nanoparticle. The inner field can be represented as

$$\mathbf{E}_{in} = f_1(r,\theta)\cos\varphi\hat{r} + f_2(r,\theta)\cos\varphi\hat{\theta} + f_3(r,\theta)\sin\varphi\hat{\varphi}. \tag{4}$$

Cartesian components of the FW electric field and the induced nonlinear current contain different terms, which are proportional to $e^{im\varphi}$. Parity of momentum projection m in generated multipoles is defined by the dependence of the nonlinear current on azimuth angle φ. After some algebra, we find that in the spherical coordinate system, components of two types of the nonlinear current contain only even or odd values of m, as specified in Table I.

Table 1. Values of m for the nonlinear current in the spherical coordinate system

	$J_{odd,r,\theta,\varphi}$	$J_{even,r,\theta,\varphi}$
m	$\pm1,\pm3,\pm5$	$0,\pm2,\pm4$

We then perform direct numerical modeling of SHG from a GaAs nanocylinder illuminated by plane wave in vacuum. Figure 2(a) shows the calculated dependence of SHG efficiency on the rotation angle, defined as the ratio of the total SH radiated power to the energy flux of the fundamental wave through the geometrical cross section of the particle. Interestingly, the SHG radiation follows the threefold symmetry of the zinc-blende lattice with regard to the (111) direction resulting in radiation patterns repeating every 60° when varying the pump polarization as shown in bottom inset of Fig. 2(a). The conversion efficiency, however, remains independent of angle in agreement with experimental results shown in Fig. 2(b) featuring a multipeaked structure governed by a hierarchy of Mie-like resonances (2). In the multipolar expansion of SHG, we obtain that the nonlinear current $\mathbf{J}_{even}$ generates an electric dipole $a_E(1,0)$, an electric quadrupole $a_E(2,0)$ electric octupoles $a_E(3,0)$ and $a_E(3,2) = a_E(3,-2)$, magnetic quadrupoles $a_M(2,2) = -a_M(2,-2)$ and magnetic octupoles $a_M(3,2) = -a_M(3,-2)$, while the nonlinear current $\mathbf{J}_{odd}$ generates electric dipole $a_E(1,1) = a_E(1,-1)$, electric quadrupoles $a_E(2,1) = a_E(2,-1)$, electric octupoles $a_E(3,1) = a_E(3,-1)$, magnetic dipoles $a_M(1,1) = -a_M(1,-1)$, magnetic quadrupoles $a_M(2,1) = -a_M(2,-1)$, magnetic octupoles $a_M(3,1) = -a_M(3,-1)$.

3.1. SHG power and radiation pattern

SH electric and magnetic fields outside the scatterer can be written as a sum over multipolar contributions. At long distances from the particle, the fields take the following form:

$$\mathbf{E}^{(2\omega)} \approx E_0 \sum_{l=1}^{\infty}\sum_{m=-l}^{l} -i\sqrt{\pi(2l+1)}\Big\{a_M(l,m)\mathbf{X}_{lm}(\theta,\varphi) + ia_E(l,m)\hat{r}\times\mathbf{X}_{lm}(\theta,\varphi)\Big\}\frac{e^{ikr}}{kr}, \quad \mathbf{H}^{(2\omega)} \approx \frac{1}{\eta}\hat{r}\times\mathbf{E}_s, \tag{5}$$

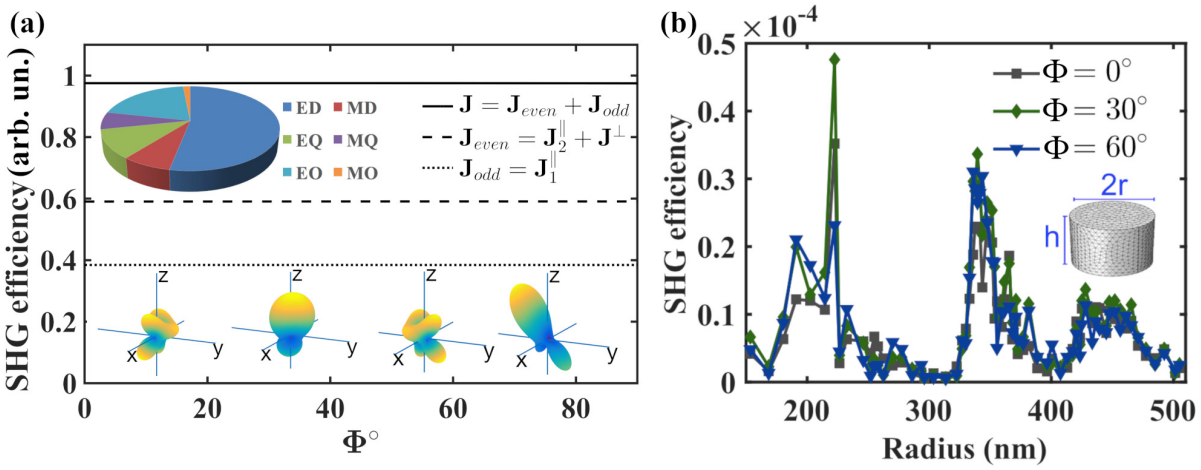

Figure 2. (a) Dependence of SHG efficiency on the pump polarization angle Φ calculated for a (111) GaAs nanocylinder with radius $r = 200$ nm and height $h = 400$ nm in vacuum. The top inset shows the multipolar decomposition of the SHG radiation idependent of the rotation angle. Bottom insets show simulated SHG patterns at $\Phi = 0°, 30°, 60°$, 90°; (b) Measured SHG efficiency vs nanocylinder radius at $\Phi = 0°, 30°, 60°$ as indicated by color curves. The SH signal integrated over all polarizations was collected in transmission using a 0.9 NA objective.

where wavenumber $k = k(2\omega)$, vacuum impedance $\eta = \sqrt{\mu_0/\varepsilon_0}$. Using the Poynting vector $\mathbf{S}^{(2\omega)} = \frac{1}{2}\mathrm{Re}\left(\mathbf{E}^{(2\omega)} \times \mathbf{H}^{*(2\omega)}\right)$, we write the expression for the far-field diagram distinguishing contributions of even and odd multipoles generated by the nonlinear currents $\mathbf{J}_{even}$ and $\mathbf{J}_{odd}$:

$$F(\theta,\varphi) = S_r r^2 = \left\{ \frac{1}{2\eta}\left(|\mathbf{E}^{(2\omega)}_{even}|^2 + |\mathbf{E}^{(2\omega)}_{odd}|^2\right) + \frac{1}{2}\mathrm{Re}\left(\mathbf{E}^{(2\omega)}_{even} \times \mathbf{H}^{*(2\omega)}_{odd} + \mathbf{E}^{(2\omega)}_{odd} \times \mathbf{H}^{*(2\omega)}_{even}\right)\right\} r^2 . \quad (6)$$

The far-field diagram (6) depends on the rotation angle, while the total SHG-power does not change if the polarization of the incident plane wave rotates. The last two terms are proportional to $e^{\pm i(m'-m'')\varphi}$, where m' is even and m'' is odd. They do not contribute to the total SH power because the integrals of them over angle φ are equal to zero. Thus, the extent to which different multipole orders contribute to a certain current configuration is independent of the pump polarization. In contrast, the angular distribution within a given order varies.

The described remarkable far-field properties allow designing nonlinear nanoantennas with radiation patterns that can be manipulated by changing the pump polarization while maintaining a constant conversion efficiency.

The work was supported by the Russian Foundation for Basic Research (Grants No. 18-02-00381, 19-02-00261). Modeling was supported by the Russian Science Foundation (Grant No. 17-12-01574).

References

[1] Smirnova D A and Kivshar Y S 2016 Multipolar nonlinear nanophotonics, *Optica* **3** 11

[2] Frizyuk K, Volkovskaya I, Smirnova D, Poddubny A and Petrov M 2019 Second-harmonic generation in Mie-resonant dielectric nanoparticles made of noncentrosymmetric materials, *Phys. Rev. B* **99** 075425

[3] Smirnova D A, Smirnov A I and Kivshar Y S 2018 Multipolar second-harmonic generation by Mie-resonant dielectric nanoparticles, *Phys. Rev. A* **97** 1 013807